Correspondence to:
F. Di Mare,
f.d.mare@fys.uio.no

Turbulence and Intermittency in the Winter Cusp Ionosphere Studied With the ICI Sounding Rockets

F. Di Mare[1] , **A. Spicher[1,2]** , **L. B. N. Clausen[1]** , **W. J. Miloch[1]** , and **J. I. Moen[1,3]**

[1]Department of Physics, University of Oslo, Oslo, Norway, [2]Department of Physics and Technology, the Artic University of Norway, Tromsø, Norway, [3]University Centre in Svalbard, Longyearbyen, Norway

Abstract The characteristics of turbulent plasma in the winter cusp ionosphere is studied based on in-situ data from the Investigation of Cusp Irregularities (ICI) sounding rockets. The electron density fluctuations from ICI-2 and ICI-3 missions have been analyzed for the whole flight, using advanced time-series analysis techniques. The analysis of the autocorrelation scale is indicative of the turbulence integral scale and marks the onset of the turbulent cascade from large to small scales in the power spectrum density of the rocket data. The power spectrum is typical for a turbulent field. The turbulent structures are persistent in the data, which are quantified by analyzing the Probability Distribution Functions (PDFs) and their deviations from the Gaussian distribution. The kurtosis analysis indicates the presence of intermittency. These results are compared with the Local Intermittence Measure - LIM, which confirms the presence of small scale intermittent structures. The turbulence measured by rockets appears well developed and covers frequencies between 1 Hz and several hundred Hz. There is a good agreement with the previous results, suggesting that density fluctuations in the ionospheric cusp agree with the turbulence framework in which intermittent processes transfer energy across different scales.

1. Introduction

Space plasmas display fluctuations and nonlinear behavior at a broad range of scales, and in most cases they are in a turbulent state (Bruno & Carbone, 2013; Frisch, 1995; Tu & Marsch, 1995). Despite of many studies and recent advances in research, many questions related to space plasma turbulence are still open. Here, we focus on the cusp ionosphere, where the coupling with the magnetosphere and the solar wind leads to highly dynamic phenomena resulting in plasma irregularities (Kelley, 2009). High-latitude F region is characterized by irregularities, instabilities, and turbulence (Basu et al., 1994; Carlson et al., 2007; Moen et al., 2000, 2002, 2002; Oksavik et al., 2012), which cover a wide range of scales, from hundreds of kilometers to a few meters (e.g., Carlson et al., 2007; Tsunoda, 1988). Their presence is considered customarily in the F region ionosphere. Such irregularities are important aspect of the space weather, and they can disturb the propagation of trans-ionospheric radio waves, which might impact the increasing human activity in the polar regions, which often relies on such signals (Bothmer & Daglis, 2007; Carlson, 2012; Moen et al., 2013).

Power spectra are powerful tools in the analysis of turbulence, and they allow to describe how the main energy cascade develops (Alexandrova et al., 2009; Frisch, 1995; Leamon et al., 1998; Tu et al., 1989). Ionospheric plasma turbulence and irregularities should be described by power laws (Kintner & Seyler, 1985; Tsunoda, 1988) and a double-slope spectra seem to be common in the high-latitude F layer plasma (Ivarsen et al., 2019; Mounir et al., 1991; Spicher et al., 2014; Villain et al., 1986). The same behavior is well documented at low-latitude (e.g., Hysell et al., 1986; Jahn & Labelle, 1998; Kelley et al., 1982; LaBelle et al., 1986). Several mechanisms are often associated with the spectra observed: the Gradient Drift Instability (GDI) (Cerisier et al., 1985; Mounir et al., 1991), due to the differential drifts of ions and electrons on a plasma density gradient; the presence of strong flow shears suggests the Kelvin-Helmholtz instability (KHI) as a possible candidate for the generation of plasma irregularities in the polar regions (Basu et al., 1990; Carlson, 2012; Carlson et al., 2007). Indeed, Basu et al. (1988) showed a tendency for intense irregularities at large scales, likely due to KHI, to arise in regions with velocity shears. Past observations (e.g., Basu et al., 1988, 1990; Kintner & Seyler, 1985) displayed a slope $\alpha = -5/3 \approx -1.67$ for the power spectra of the electron density fluctuations, both for the GDI and the KHI, which is in agreement with linear theory. Basu et al. (1984), Villain et al. (1986), Mounir et al. (1991), Spicher et al. (2014) presented direct evidence of a steepening of the spectra at high frequencies measured in the high-latitude F region auroral zone and cusp region. Such

dual-slope spectra may indicate the presence of two different physical regimes, one where low-frequency processes are dominating and one where kinetic effects become important.

With the aim to provide an extensive analysis of features of the plasma turbulence in the cusp ionosphere, data from the ICI-2 and ICI-3 sounding rocket experiments in the high-latitude F-region ionosphere have been analyzed. In this paper, we carry out advanced time series analysis to characterize turbulence and evaluate its statistical properties including intermittency (Bruno et al., 2001; Sorriso-Valvo et al., 1999). For the analysis, we use several tools to address different aspects of turbulence characteristics, and will show that in case of this well-developed turbulence, intermittency can be considered an important mechanism for the energy transfer across different scales.

2. The ICI Data Missions

Sounding rockets can place scientific instruments on board to measure directly specific regions of the ionosphere. This allows to collect unique science data. With the possibility to be launched on-demand where and when phenomena of interest are occurring, in-situ sounding rocket measurements are the most feasible approach to describe the nature of the plasma structures under various conditions and to provide the plasma parameters needed to properly evaluate existing models for plasma instabilities. The Investigation of Cusp Irregularities - ICI sounding rockets are a series of Norwegian rocket experiments that aim to study irregularities and turbulence in the ionospheric cusp. The high-resolution measurements of the absolute electron density provided by the multi-Needle Langmuir Probe (m-NLP) (Bekkeng et al., 2010) has allowed to advance in knowledge by increasing the spatial resolution of the absolute density measurements from kilometers scales to below-meter scales.

2.1. The ICI-2 Sounding Rocket Mission

The ICI-2 sounding rocket was launched into the cusp ionosphere at 10:35:10 UT on 5 December 2008 from Ny-Ålesund, Svalbard (NYA: 78.9°N, 11.9°E geographic coordinates), and the payload reached apogee in its nominal trajectory at 328.7 km altitude after 302 s flight time. The rocket flew almost perpendicular to the Earth's magnetic field and encountered large plasma density enhancements. Details about the space environment during the flight and the plasma conditions can be found in Lorentzen et al. (2010).

In this study, we use data from the four-needle Langmuir probe (m-NLP), deployed on booms perpendicular to the ICI-2 payload body (Bekkeng et al., 2010; Jacobsen et al., 2010), with a sampling rate of 5,787 Hz. Figure 1a) displays the electron density N_e measured with respect to the time of flight t. The spin modulation due to the rotation of the spacecraft was removed (Jacobsen et al., 2010). The maximum values ($N_e \approx 1.1 \times 10^{-11} \mathrm{m}^{-3}$) are reached early in the flight at about $t = 130$ s that corresponds to altitude $h = 200$ km. Then the density drops to about $N_e \approx 0.5 \times 10^{-11} \mathrm{m}^{-3}$ and throughout the remainder of the flight, several large-scale density enhancements are observed. Around the time intervals $\Delta t \approx [180, 240]$ s and $\Delta t \approx [380, 430]$ s of the flight, the electron density varies between $0.5 \times 10^{-11} \mathrm{m}^{-3}$ and $1 \cdot 10^{-11} \mathrm{m}^{-3}$. Figure 1b shows the corresponding spectrogram of the electron density fluctuations $\Delta N_e / N_e$, which is obtained with a Hamming window over four seconds intervals with 75 % overlapping. The horizontal lines are associated with the spin of the payload and its harmonics. As can be seen, enhanced power spectral density (PSD) ranging from 1 Hz to several hundreds of Hz occurs in distinct regions in relation to the larger-scale structures above-mentioned. Using the relative motion between the plasma and the rocket, this may correspond to spatial scales smaller than 10 m (Oksavik et al., 2012).

2.2. The ICI-3 Sounding Rocket Mission

The ICI-3 mission was launched from Ny-Ålesund (NYA: 78.9°N, 11.9°E, geographic coordinates) at 07:21:31 UT on December 3, 2011 into the cusp ionosphere, where the payload reached an apogee of 354.5 km at the time of the flight $t = 312.9$ s. In the ICI-3 mission three spherical and five m-NLPs were mounted on booms which were deployed perpendicular to the payload body with a sampling rate of 8680.5 Hz. Figure 2a shows the electron density measured by m-NLP with respect to time of flight, between $t = 150$s ($h = 236.8$km)
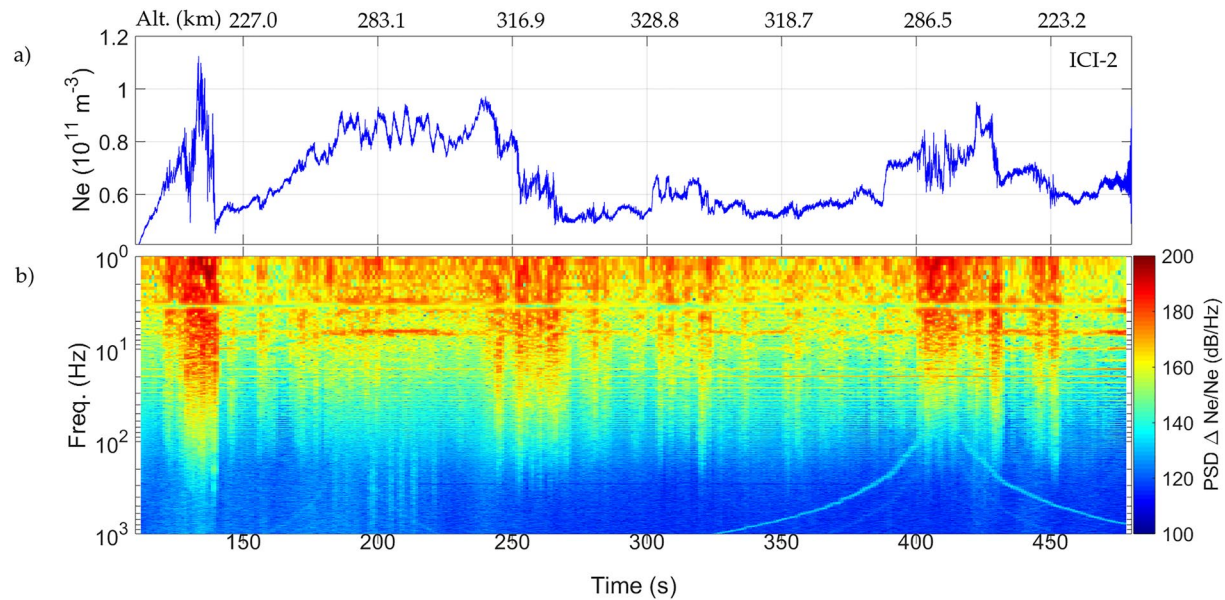
Figure 1. (a) Electron density measured by m-NLP during the ICI-2 mission. (b) Spectrogram of the electron density fluctuations. The plots are given as a function of time of flight and the corresponding altitude.

and $t = 500\,s$ ($h = 202.8$km), and using three of the probes (Spicher et al., 2016). The electron density N_e is about three times larger than the one observed during the ICI-2 flight and varies significantly during the entire flight. Figure 2b shows the corresponding spectrogram of the ICI-3 electron density fluctuations $\Delta N_e / N_e$. The spectrogram was computed in as similar way as for Figure 1. We observe significant PSD reaching several hundred Hz throughout the flight up to 1 kHz frequencies. An obvious difference between ICI-2 and ICI-3 is that ICI-2 exhibits enhanced PSD at high frequencies only several localized intervals during the flight, while this roughly continuous for ICI-3.
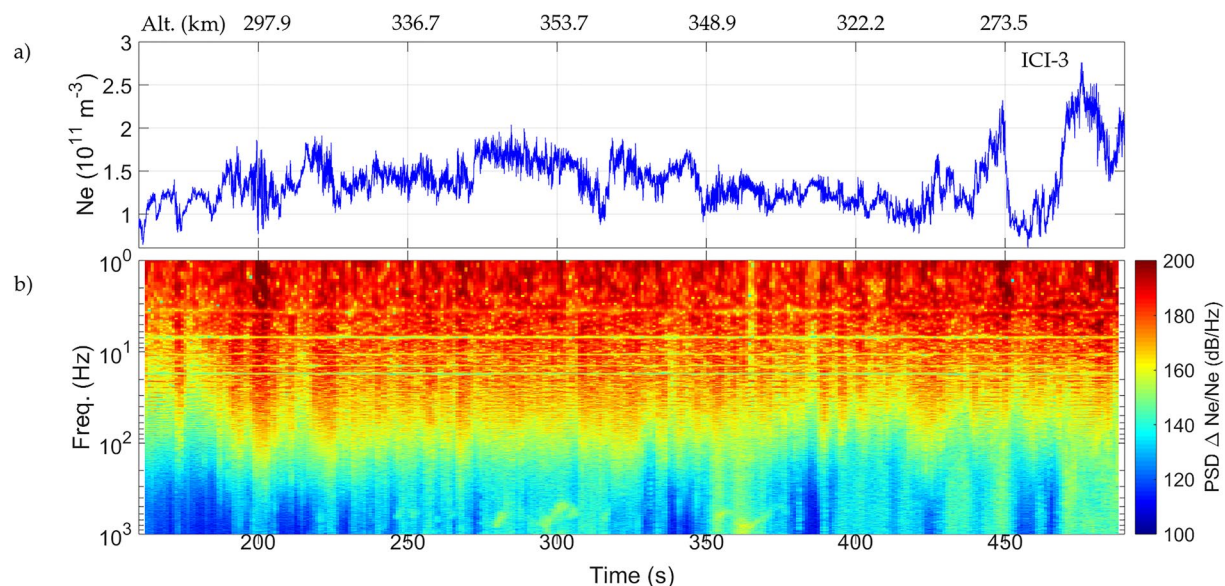

Figure 2. (a) Electron density measured by m-NLP during ICI-3 mission. (b) Spectrogram of the electron density fluctuations. The plots are given as a function of time of flight and the corresponding altitude.
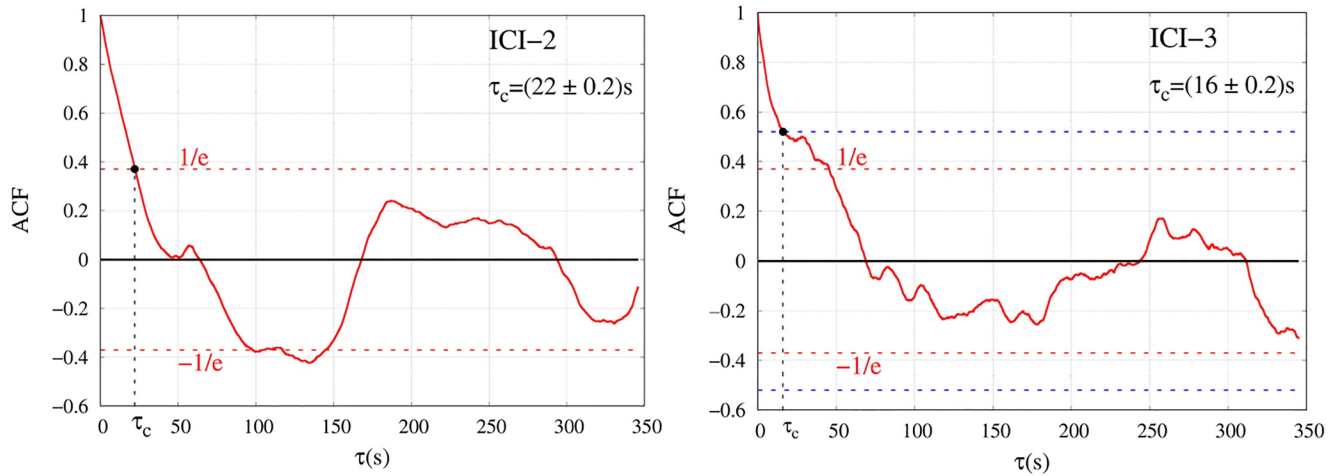
Figure 3. The autocorrelation function (ACF) of the electron density measured by ICI-2 (left panel) and ICI-3 (right panel) as a function of τ.

3. Observations

In order to characterize the properties of the plasma, the electron density has been analyzed using several tools: the autocorrelation function, which gives useful information about the correlation scale of the field; the energy power spectrum, which indicates how the energy is transferred between different scales; the Probability Distribution Functions (PDFs) of the scale-dependent increments, whose deviation from Gaussian will qualitatively illustrate the presence of intermittency; the fourth-order moment, the kurtosis, is able to measure the flatness or peakedness of a distribution compared to a Gaussian, and the Local Intermittency Measure (LIM), that helps in identifying the presence of intermittent structures. The time series shown in Figure 1 for ICI-2 and in Figure 2 for ICI-3 were used for the analysis, specifically, the time period 110 s ≤ t ≤ 480 and 160 s ≤ t ≤ 490 s, respectively.

3.1. Autocorrelation Function

The autocorrelation function (ACF) defines how data points in a time series are related, on average, to the preceding data points (Box et al., 1994), that is, in this context $ACF = \langle [N_e(t) - \langle N_e \rangle][N_e(t + \tau) - \langle N_e \rangle] \rangle / \sigma$, where σ is the standard deviation of N_e, $N_e(t)$ is the time series representative of the electron density and τ is the separation time scale. Here $\langle \ldots \rangle$ is an ensemble average that is, equivalent to a suitably chosen time- or space-averaging procedure. The ACF can test the self-similarity of the signal over different lag times. We estimate the correlation time of plasma density τ_c, which may help identifying the integral length scale of turbulence. It represents the largest separation distance over which eddies are still correlated, that is, the largest turbulent eddy size (Matthaeus et al., 2005). Figure 3 shows the ACF versus time scale τ for the electron density fluctuations of ICI-2 and ICI-3 data.

Both cases display a roughly parabolic decay near the origin, as observed in the solar wind turbulence (Matthaeus & Goldstein, 1982). The uncorrelated-scale noise level is reached when the ACF starts fluctuating around zero. The noise level is delimited by the horizontal red dashed lines, corresponding to the values $\pm 1 / e$, as customary used in the evaluation of the correlation scale in turbulent phenomena (Bruno & Carbone, 2013). The correlation scale τ_c is defined as time scale at which the ACF intersects the bands that delimit the noise level. While for ICI-2 $\tau_c = (22 \pm 0.2)$ s and the noise level is well contained between the values $\pm 1 / e$, for ICI-3 there are small fluctuations outside the noise band, that is, they are before the ACF reaches the horizontal line $+1 / e$. In the right panel, the additional blue dashed line above and below the red-line limits, have been inserted to include the fluctuations and enlarge the noise bands. Thus for ICI-3, $\tau_c = (16 \pm 0.2)$ s.
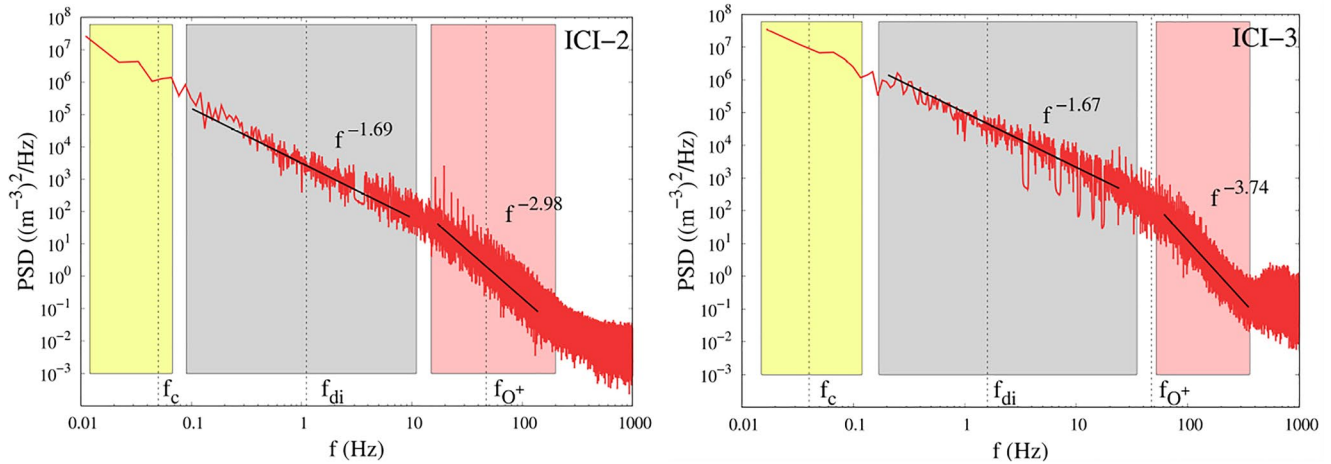
Figure 4. The power spectral density (PSD) of electron densities of ICI-2 (left panel) and ICI-3 missions (right panel). The vertical black dashed lines indicate the frequency related to the correlation time f_c, the frequency related to the ion inertial length f_{di}, and the gyrofrequency of oxygen ions in the polar ionosphere f_{O^+}.

3.2. Power Spectra

Power spectra provide information about the scaling properties of the field fluctuations. Figure 4 displays the power spectral density (PSD) of ICI-2 (left panel) and ICI-3 (right panel) data. With the aim to represent how the turbulent cascade develops, we include three characteristic frequencies in the spectrum that delimit different ranges of the turbulent regime. From the phenomenological point of view, Kolmogorov (1941) claims the presence of three separate ranges in the energy spectrum: an injection range, which corresponds to the large scales of turbulent motions, denoted the driving scale; an inertial range, where nonlinear interactions serve to transfer energy from large to smaller scales; finally a dissipative range, that in which the energy dissipates. We show these three ranges to assess how the different ranges of the turbulent cascade may apply to our ionospheric system. On the left side of both panels in Figure 4 we indicate $f_c \approx 1 / \tau_c$, which readily relate to the corresponding autocorrelation times, where we identify the beginning of the turbulent cascade at large scales/small frequencies (yellow zone) that delimits the onset of the inertial range (gray zone). Here a process of fragmentation at large-scale can developed (Kolmogorov, 1941). We find f_{di}, which is the frequency related to the ion inertial length $d_i = c / \omega_{pi} \simeq (600 - 900)$ m, where c is the speed of light and ω_{pi} is the ion plasma frequency, averaged for the flight used. By inserting the appropriate values we obtain: $f_{di} \simeq 1.1$ Hz for ICI-2 and 1.6 Hz for ICI-3. Last, to the right, the frequency $f_{O^+} \approx 47$ Hz, is the gyrofrequency of oxygen ions in the polar ionosphere (the Earth's magnetic field $B \approx 5 \cdot 10^{-5}$ T for both flights). We note that the ICI-2 and ICI-3 power spectra have a break around $f \in (15 - 47)$ Hz. These values are located reasonably between the frequencies corresponding to the ion inertial length and the gyrofrequency of oxygen ions f_{O^+}, where the kinetic plasma effects are believed to start being non-negligible (red zone), or where diffusion, drift waves (LaBelle et al., 1986), or wave steepening (Hysell et al., 1986) observed at equatorial regions can be also relevant for the polar plasma dynamics. Both spectra exhibit a clear double-slope spectrum with $\alpha_1 = -1.69$ at lower frequencies and $\alpha_2 = -2.98$ at higher frequencies for ICI-2. Similar values are found for ICI-3: $\alpha_1 = -1.67$ and $\alpha_2 = -3.74$. The latter slope α_2 appears steeper than that of the electron density of ICI-2. These results are in a good agreement with previous studies in literature (Basu et al., 1990; Mounir et al., 1991; Spicher et al., 2014; Villain et al., 1986). Spacecraft and sounding rocket data commonly have a weakly stationary nature, which is visualized as a certain regularity in the time series and characterized by a constant mean and an autocorrelation function that are not dependent on the absolute time, but on the time difference τ between measurements (Jenkins & Watts, 1968; Pécseli, 2000; Spicher et al., 2015). Validation of the stationary nature of several intervals of the time series here used can be found in Spicher et al. (2014, 2015). To verify the results obtained with the power spectra calculation, which requires that data are locally stationary, we calculated the spectra at a higher cadence (at every 60 s), demonstrating how the energy cascade typically described by a double slope continues to persist. Table 1 summarizes results for

Table 1
Spectral Indices of the Power Spectra Estimated for Time Intervals of 60 s Each

ICI-2 mission		
Time interval	α_1	α_2
(120–180) s	−1.67	−2.98
(180–240) s	−1.69	−2.86
(240–300) s	−1.66	−2.98
(300–360) s	−1.69	−3.08
(360–420) s	−1.69	−2.88
(420–480) s	−1.65	−2.98
ICI-3 mission		
Time interval	α_1	α_2
(170–230) s	−1.64	−3.68
(230–290) s	−1.62	−3.66
(290–350) s	−1.62	−3.74
(350–410) s	−1.64	−3.68
(410–470) s	−1.67	−3.71

Note: Spectral indices α_1 and α_2 and correspond to the low- and high-frequency ranges, respectively.

spectral indices α_1 and α_2 corresponding to the low- and high-frequency ranges, estimated for time intervals of 60 s each. The slope at the lower frequencies remains consistent with Kolmogorov's law. The same applies at higher frequencies, where the values of the slope remain very close to those of the whole.

3.3. Intermittency

The statistics of turbulent fluid flows can be characterized by the Probability Distribution Function (PDF) over varying scales (Frisch, 1995). For intermittent signals, it is observed that PDFs are scale-dependent. At large scales the behavior is approximately Gaussian, and as the scale decreases, the wings of the distribution become increasingly stretched leading to large deviations from the Gaussian (Sorriso-Valvo et al., 1999). The Gaussianity threshold may be linked to the change of topology of the energy transfer. This implies that intense fluctuations have a higher probability of occurrence than that they should have if they had Gaussian distribution (Bruno & Carbone, 2013). This scaling dependence of PDF can be taken as a definition of inter-mittency (Bruno & Carbone, 2013). We calculate the PDF of increments ΔN_e at different scales τ, standard-ized by normalizing to their standard deviation σ. Figure 5 shows the PDF at different time scales and the black dashed line represents a reference Gaussian distribution. At large scales PDF displays a shape close to Gaussian. This behavior is well observed for ICI-3 at large scales $\tau = 30.145$ s and $\tau = 3.768$ s, while it is less clear for ICI-2. Then PDF becomes more and more stretched as τ decreases (Bruno & Carbone, 2013), and deviation from Gaussian curve is observed in both datasets, although the effect is more evident for ICI-3.

A way to quantify the deviation from a Gaussian distribution is the normalized fourth-order mo-ment of the increments, the kurtosis (or flatness) $K = \left\langle S_\tau^4 \right\rangle / \left\langle S_\tau^2 \right\rangle^2$, where τ is the scale of interest and $S_\tau^p = \left\langle | N_e(t + \tau) - N_e(t) |^p \right\rangle$ is the structure function of order p of the time series of density measurements $N_e(t)$ (Bruno & Carbone, 2013). The behavior of this parameter at different scales gives an estimate of the degree of intermittency of a turbulent system, as suggested by Frisch (1995). When the time series are dominated by intermittent extreme events, we expect high kurtosis according to theory (Frisch, 1995). As we can observe in Figure 6, the kurtosis initially fluctuates around the Gaussian value $K = 3$ at large scales, roughly down to the correlation scale, and then increases as a power law $K(l) \sim l^\kappa$. The power-law fitting range is generally consistent with the spectral inertial range, slightly shifted toward smaller scales, bounded
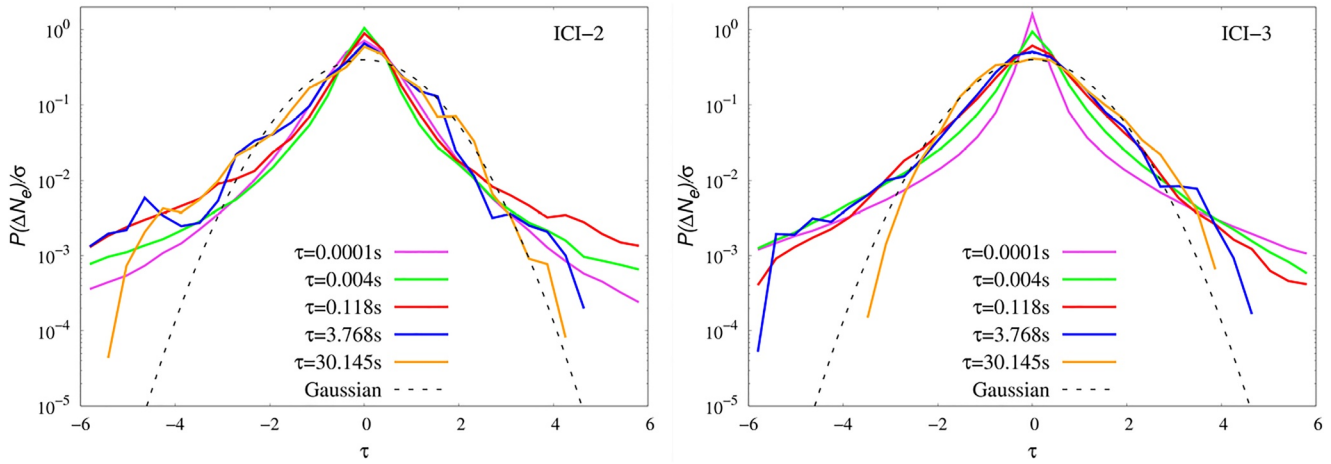
Figure 5. Probability distribution functions of the normalized increments $\Delta N_e^{(\tau)} / \sigma$ at different time scales τ. The black dotted line is a Gaussian distribution plotted here as a reference.

by the time related to ion inertial length τ_{d_i} and the time associated with the gyrofrequency of oxygen ions $\tau_{O^+} = 1 / f^{O^+} = 0.02$ Hz. These values correspond to the frequencies inserted in the power spectra in order to achieve direct correspondence between different analysis tools employed. The scaling exponent κ gives a quantitative estimate of the intermittency, that is, of the anomalous scaling of the field fluctuations (Sreenivasan & Antonia, 1997). This value is $\kappa \approx -0.358$ for ICI-2 and -0.369 for ICI-3. The kurtosis K for ICI-2 data shows one decade of large-scale fluctuations around the value $K = 3$ and then it increases when going toward smaller time scales and tends to saturate. For ICI-3 instead, after an initial oscillation around the Gaussian value that covers two decades, the growth of the kurtosis is more gentle and the saturation level is not observed.

To support the observations of the presence of intermittent structures, we calculate the Local Intermittency Measure (LIM) introduced by Farge et al. (1990). LIM represents the energy content of fluctuations at a specified scale s and at specified time t_0 with respect to the average power at that scale or with simple words, the local activity of the signal at each scale s (Consolini & De Michelis, 2005; Farge, 1992):

$$LIM_{s,t_0} = \frac{|w_s(t_0)|^2}{\left\langle |w_s(t)|^2 \right\rangle_t}$$
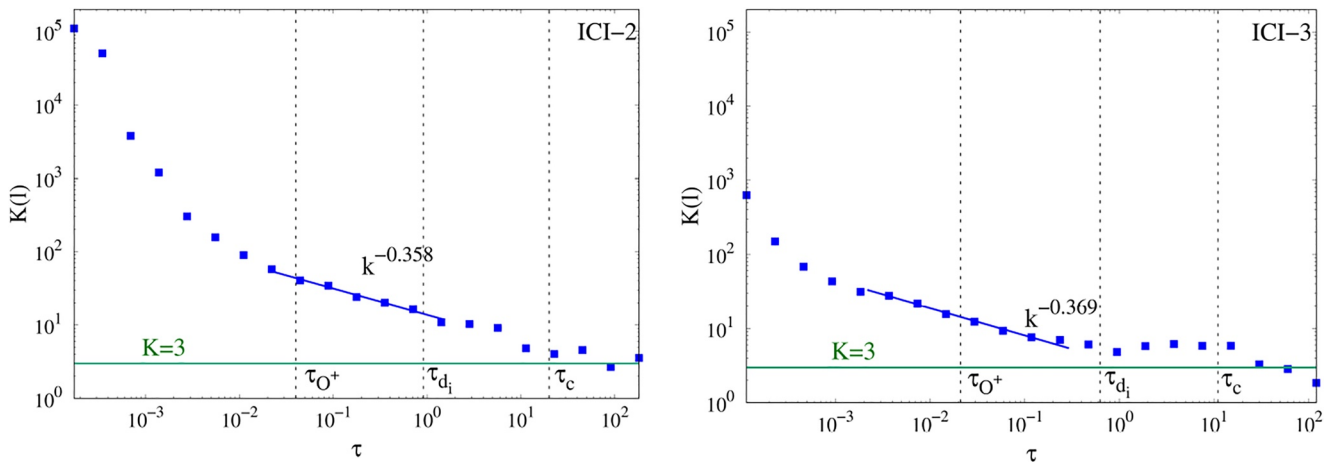
Figure 6. The kurtosis of the electron density fluctuations calculated using ICI-2 (left panel) and ICI-3 data (right panel), as well as the power-law fit for the two cases. The horizontal solid green line indicates the Gaussian value $K = 3$; The vertical black dashed lines indicate the gyro-period related to the gyrofrequency of oxygen ions, the inertial period τ_{di} related to the frequency f_{di}, and the correlation time τ_c.
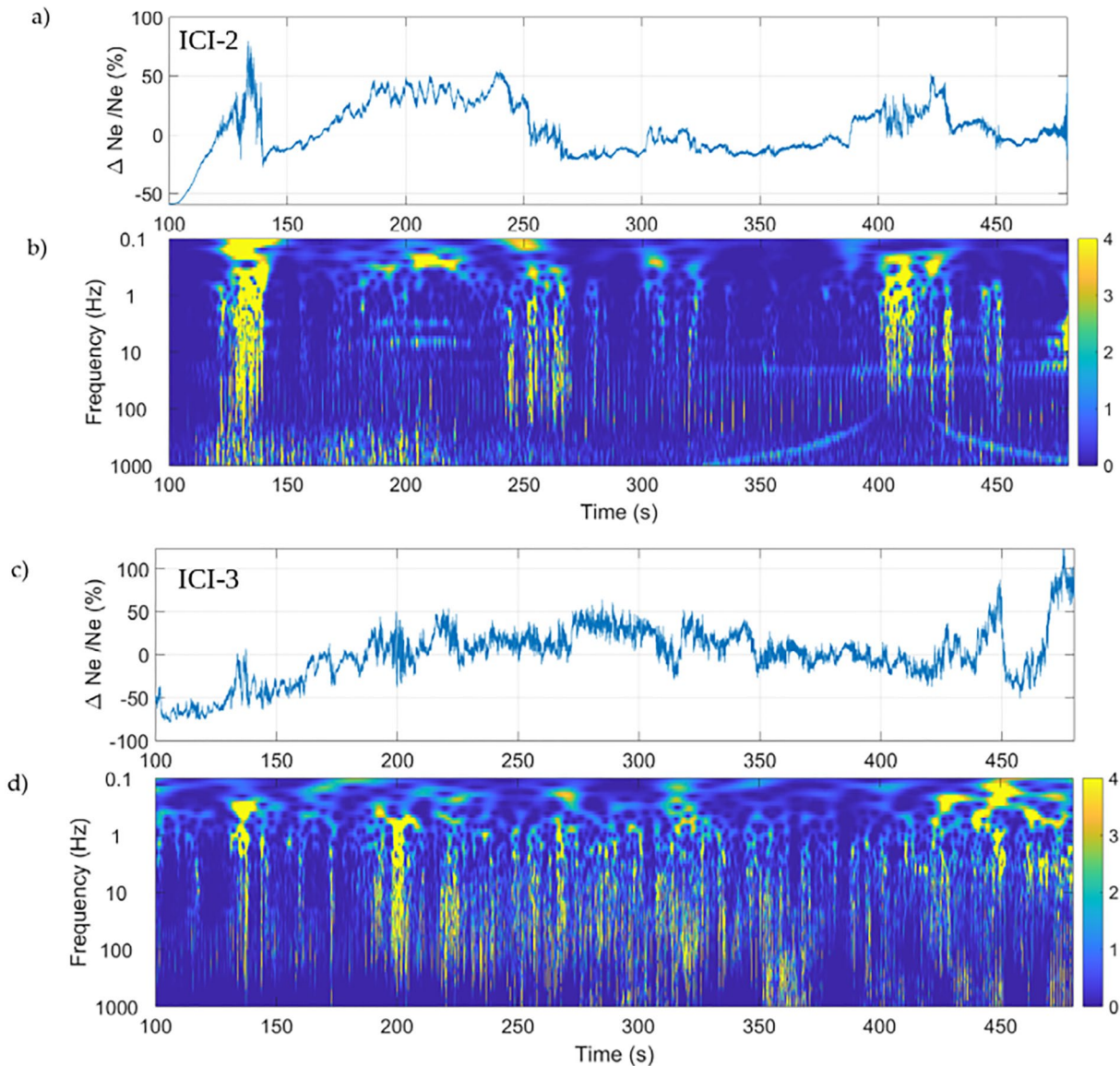
Figure 7. LIM analysis of the electron density data. (a and c) The electron density data for ICI-2 and ICI-3 respectively. (b and d) LIM analysis given as a function of time of flight for ICI-2 and ICI-3 and LIM intensity in arbitrary units (see color bar).

where $|w_s(t_0)|^2$ is the local energy density at the scale s, $\langle |w_s(t)|^2 \rangle_t$ corresponds to the averaging over time at the same scale s and $w_s(t)$ are the wavelet coefficients for the electron density at scales s and time t (Consolini & De Michelis, 2005; Farge, 1992; Tam et al., 2005). This technique is used to identify intermittent events and is able to estimate the degree of irregularity at different scales. The global wavelet energy spectrum corresponds to the Fourier energy spectrum smoothed by the wavelet spectrum at each scale (Farge et al., 1990). In this work the LIM is obtained using wavelet coefficient calculations based on the Morlet wavelet and adapted from a software provided by Torrence and Compo (1988). Figures 7a and 7c show the electron density fluctuations and the corresponding LIMs are presented in Figures 7b and 7d. For ICI-2, we observe large-scale structures, which extend into small-scale structures in several time intervals: $125 \leq t \leq 140$ s, $190 \leq t \leq 225$ s, $240 \leq t \leq 260$ s, $310 \leq t \leq 330$ s and between $400 \leq t \leq 440$ s. Structures at frequencies ≤ 1 Hz and up to 100 Hz are observed in the time intervals indicated above, while between 120 and 240 s the small scale structures reach frequencies up to 1 kHz. For ICI-3, we observe different characteristics of LIM (see again Figure 7d). Large scale irregularities with frequencies between 0.1 and 1 Hz are observed at times of flight of approx. 140, 170, 200, 220, 270, 320 s and in the final part of the series between

440 and 500 s. In the latter case, intermittent structures cover frequencies up to 1,000 Hz for almost all the time interval mentioned above. This is in agreement with the statistical analysis conducted so far which asserts the presence of a developed turbulence during both flights.

4. Discussion

Through studies of turbulence characteristics, some phenomenological considerations about the energy transfer and its distribution in a system can be made. The development of turbulence and irregularities occurs when free energy is redistributed through some instability mechanism and, consequently, both the source of energy and the instability are coupled (Treuman & Baumjohann, 1997). The density gradients (usually associated with the polar cap patches), flow shears and particle precipitation (Carlson, 2012; M. Keskinen & Ossakow, 1983; Moen et al., 2013; Tsunoda, 1988) are the three sources of free energy believed to be dominant in the polar regions. With large-scale variations in the configuration space in the ionosphere, there are associated macro-instability processes such as the gradient drift instability (GDI) (e.g., Linson & Workman, 1970) and Kelvin-Helmholtz instability (KHI) (M. J. Keskinen et al., 1988). Once the energy is injected at large scales, the non-linear processes are activated, producing a continuous transfer of energy across scales. From the phenomenological point of view, this corresponds to a process of fragmentation of large-scale turbulent structures which, by breaking up, produce turbulent structures at smaller scales.

The autocorrelation function (ACF) allows for evaluating the scales at which the turbulent structures are identified. In our analysis, the behavior of the ACF is typical of turbulent fields, that is, it has a roughly parabolic shape near the origin, indicating the field smoothness in the dissipative range, followed by a slower decay toward zero, indicative of the inertial range of turbulence (Pope, 2000). We found values of the correlation time $t = 22$ s and $t = 16$ s for ICI-2 and ICI-3 electron density respectively, corresponding to structures with scales of tens kilometers. This may be related to the integral length scale of turbulence in our ionospheric system that represents the largest separation distance over which eddies are still correlated, that is, the largest turbulent eddy size (Bruno & Carbone, 2013). This is in agreement with the spatial scale of individual irregularities found in Basu et al. (1990), that can range from tens of km down to meters. By assuming that Taylor's hypothesis is satisfied and the turbulence is purely spatial and it is isotropic in the direction perpendicular to the magnetic field, the frequencies of the spectra may be related to the wavelengths when the relative motion of the plasma with respect to the rocket is known (Taylor, 1938). The correlation time value has been inserted into the frequency PSD through suitable transformations and, as expected, it is placed in the initial ranges of the spectrum, where the energy cascade is assumed to begin.

One can see that the spectra have similar shapes for both sounding rocket experiments. The spectra intensities are similar at low frequencies, but different at high-frequencies. We can clearly recognize two power-laws present in the spectra: at low frequencies, the spectra display $\alpha_1 = -5/3 \simeq -1.7$ consistent with Kolmogorov's law, then a break appears in the interval $f \in (15 - 47\text{Hz})$. These values lay reasonably between the frequency corresponding to the ion inertial length and the gyrofrequency of the oxygen ions f_{O^+}, where the kinetic plasma effects are believed to start being non-negligible (red zone), or where diffusion, drift waves (LaBelle et al., 1986), or wave steepening (Hysell et al., 1986) observed at equatorial regions can be also relevant for the polar plasma dynamics. We estimate that the steepening of the spectra corresponds to wavelengths $\lambda \in (21,66)$ m. This is significantly larger than the Larmor radius of the oxygen ion $r \simeq 4$ m for a typical ion temperature of $T_i \simeq 1000$ K. These findings are in agreement with results in Spicher et al. (2014). At higher frequencies, the power spectrum is $\alpha_2 = -2.98$ for ICI-2 and $\alpha_2 = -3.74$ for ICI-3. The latter slope appears steeper and suggests a more complex dynamics in the turbulent cascade in the ICI-3 mission. The PSD is larger for ICI-3 than ICI-2 until about 50 Hz (the break), indicating more irregularities at these frequencies. It is also important to point out that such results can be affected by the Doppler shift and should be considered with care (Fredricks & Coroniti, 1976).

The study of PDFs suggests the presence of coherent structures localized in space and time, showing a non-Gaussian behavior as decreasing scales. This implies that intense small scale fluctuations have high probability of occurrence and the PDFs appear as stretched exponential functions at the smallest scales. This scaling dependence of PDFs is a different way to say that the scaling exponents of fluctuations are anomalous, and they can be taken as a different definition of intermittency (Bruno & Carbone, 2013).

The kurtosis K, being the fourth order moment of the structure function, measures the flatness or peakedness of a distribution (Frisch, 1995), in comparison to a Gaussian. For a Gaussian $K = 3$ and a distribution affected by flatness has $K > 3$. A time series dominated by intermittent extreme events has high kurtosis. In our datasets, the scale-dependent kurtosis increases toward high-frequencies, implying the presence of coherent structures at the smallest scales. In the Navier–Stokes turbulence, it is often observed that the scaling exponent $\kappa \simeq -0.1$ (Anselmet et al., 1984). In our study the scaling exponent $\kappa \approx -0.358$ for ICI-2 and $\kappa \approx -0.369$ for ICI-3, which is consistent with a pronounced intermittency.

We finally studied a measure of local intermittency - LIM, as the degree of irregularity dependent on scales. LIM measures the local activity of the signal at each scale and has been widely applied to identify intermittent events in the solar wind turbulence (Bruno et al., 1999, 2001; Consolini & De Michelis, 2005). We observe turbulent structures covering the frequency range from > 1 Hz up to hundreds Hz in several regions of the ICI-2 flight. In data from ICI-3 rocket, one can instead observe the presence of large scales irregularities that gradually extend into small ones and fill most of the time series. This different behavior of the two missions can already be seen from the spectrograms in Figures 1b and 2b. ICI-2 shows enhanced power spectral density occurring in distinct regions of the flight, while ICI-3 shows a spectrogram structured during the entire flight. These observations and the results of LIM analysis suggest that a developed turbulence has been observed by both rockets, although there seem to be mechanisms during the ICI-3 rocket flight that facilitate the fragmentation of eddies toward smaller scales.

Summing up, data from the ICI-3 mission exhibit a steeper power spectrum at high frequencies, the wings of PDFs at small scales are higher and stretched exponentially more than those of the ICI-2 rocket data, implying that the ionosphere studied with the ICI-3 sounding rocket is more intermittent. High kurtosis for both missions is in agreement with the presence of intermittent structures, although the LIM of the ICI-3 dataset reveals the presence of intermittent structures that are present during almost the entire flight. This is also seen from the PSD comparing Figure 1b with the Figure 2b. This behavior may be attributed to different physical conditions encountered by the two rockets.

ICI-3 sounding rocket flew through an active region and a reversed flow event (Moen et al., 2013; Rinne et al., 2007), including precipitation and flow shears (Spicher et al., 2016, 2020). These different processes are features of the active cusp and could provide strong source of free energy for generation and evolution of various plasma instabilities. In contrary, the ICI-2 sounding rocket encountered regions of strong density gradients, which can be associated with polar cap-enhanced density regions and their trailing edges in particular (Lorentzen et al., 2010; Moen et al., 2012; Oksavik et al., 2012; Spicher et al., 2014). In the light of the results obtained, we expect that the ionospheric conditions during the ICI-3 sounding rocket flight could facilitate efficient meso-scale structures that would consequently create small-scale structures. The observed turbulence is more developed and intermittent. The investigation of these mechanisms at work is a subject of future work.

5. Conclusion

Plasma irregularities and turbulence are common in the F-region ionosphere, covering a broad range of scales, from hundreds of kilometers to a few meters. Using advanced time series analysis techniques, the data from the ICI-2 and ICI-3 sounding rocket experiments were analyzed. By applying the autocorrelation function we identified the integral scale of the turbulence in the studied ionosphere. The size of such large-scale structures is of the order of tens of kilometers. We observe double-slope power spectra, in which the autocorrelation frequency appears located at small frequencies, where the turbulent energy cascade is expected to start. At higher frequencies the ICI-3 power spectrum density reveals a steeper slope than the one observed for the ICI-2 dataset, suggesting a more developed turbulence, which can be attributed to different conditions of the experiment. The study of PDFs confirms the presence of coherent structures, showing a non-Gaussian behavior toward decreasing scales. Heavy tails are indicative of particularly intense field fluctuations and are related to the intermittent structures. This is further confirmed by the LIM analysis, which shows strips of intermittent structures at small-scales. The scaling exponent of kurtosis $\kappa \approx -0.358$ for ICI-2 and $\kappa \approx -0.369$ for ICI-3 have been calculated and can serve as a reference for future studies on the intermittency in the ionospheric cusp. This study strengthens the idea that that density fluctuations in

the ionospheric cusp seem to agree with the turbulence framework in which intermittent processes transfer energy across different scales. Using the methods presented, one can characterize the different levels of turbulence. These advanced techniques will be used to identify different drivers for the irregularities in the future works.

Data Availability Statement

The ICI-2 and ICI-3 m-NLP electron density data are openly available in NIRD RESEARCH DATA ARCHIVE at URLs: https://doi.org/10.11582/2021.00059 and https://doi.org/10.11582/2021.00060, respectively. Wavelet software was provided by C. Torrence and G. Compo, and it is available at URL: http://atoc.colorado.edu/research/wavelets/.

References

Alexandrova, O., Saur, J., Lacombe, C., Mangeney, A., Mitchell, J., Schwartz, S. J., & Robert, P. (2009). Universality of solar-wind turbulent spectrum from MHD to electron scales. *Physical Review Letters*, *103*(16). https://doi.org/10.1103/physrevlett.103.165003

Anselmet, F., Gagne, Y., Hopfinger, E. J., & Antonia, R. A. (1984). High-order velocity structure functions in turbulent shear flows. *Journal of Fluid Mechanics*, *140*(25), 63–89. https://doi.org/10.1017/s0022112084000513

Basu, S., Basu, S., Chaturvedi, P. K., & Bryant, C. M. (1994). Irregularity structures in the cusp/cleft and polar cap regions. *Radio Science*, *29*(1), 195–207. https://doi.org/10.1029/93rs01515

Basu, S., Basu, S., MacKenzie, E., Coley, W. R., Hanson, W. B., & Lin, C. S. (1984). F region electron density irregularity spectra near auroral acceleration and shear regions. *Journal of Geophysical Research*, *89*(A7), 5554–5564. https://doi.org/10.1029/ja089ia07p05554

Basu, S., Basu, S., Mackenzie, E., Fougere, P. F., Coley, W. R., Maynard, N. C., et al. (1988). Simultaneous density and electric field fluctuation spectra associated with velocity shears in the auroral oval. *Journal of Geophysical Research*, *93*(A1), 115–136. https://doi.org/10.1029/ja093ia01p00115

Basu, S., Basu, S., Mackenzie, E., Sharber, J. R., Hoegy, W. R., & Hoegy, W. R. (1990). Plasma structuring by the gradient drift instability at high-latitudes and comparison with velocity shear driven processes. *Journal of Geophysical Research*, *95*(A6), 7799–7818. https://doi.org/10.1029/ja095ia06p07799

Bekkeng, T. A., Jacobsen, K. S., Bekkeng, J. K., Pedersen, A., Lindem, T., Lebreton, J. P., & Moen, J. I. (2010). Design of a multi-needle Langmuir probe system. *Measurement Science and Technology*, *21*, 085903. https://doi.org/10.1088/0957-0233/21/8/085903

Bothmer, V., & Daglis, I. A. (2007). *Space weather: Physics and effects*. New York: Springer.

Box, G. E. P., Jenkins, G. M., & Reinsel, G. C. (1994). *Time series analysis: Forecasting and control* (3rd ed.). Upper Saddle River, NJ: Prentice Hall.

Bruno, R., Bavassano, B., Pietropaolo, E., Carbone, V., & Veltri, P. (1999). Effects of intermittency on interplanetary velocity and magnetic field fluctuations anisotropy. *Geophysical Research Letters*, *26*(20), 3185–3188. https://doi.org/10.1029/1999gl010668

Bruno, R., & Carbone, V. (2013). The solar wind as a turbulence laboratory. *Living Reviews in Solar Physics*, *10*(1), 1–208. https://doi.org/10.12942/lrsp-2013-2

Bruno, R., Carbone, V., Veltri, P., Pietropaolo, E., & Bavassano, B. (2001). Identifying intermittent events in the solar wind. *Planetary and Space Science*, *49*(12), 1201–1210. https://doi.org/10.1016/s0032-0633(01)00061-7

Carlson, H. C. (2012). Sharpening our thinking about polar cap ionospheric patch morphology, research, and mitigation techniques. *Radio Science*, *47*, RS0L21. https://doi.org/10.1029/2011rs004946

Carlson, H. C., Pedersen, T., Basu, S., Keskinen, M., & Moen, J. I. (2007). Case for a new process, not mechanism, for cusp irregularity production. *Journal of Geophysical Research*, *112*(A11), A11304. https://doi.org/10.1029/2007ja012384

Cerisier, J. C., Berthelier, J. J., & Beghin, C. (1985). Unstable density gradients in the high-latitude ionosphere. *Radio Science*, *20*(4), 755–761. https://doi.org/10.1029/rs020i004p00755

Consolini, G., & De Michelis, P. (2005). Local intermittency measure analysis of AE index: The directly driven and unloading component. *Geophysical Research Letters*, *32*, L05101. https://doi.org/10.1029/2004gl022063

Farge, M. (1992). Wavelet transforms and their applications to turbulence. *Annual Review of Fluid Mechanics*, *24*(395). https://doi.org/10.1146/annurev.fl.24.010192.002143

Farge, M., Holschneider, M., & Colonna, J. F. (1990). Wavelet analysis of coherent structures in two-dimensional turbulent flows. In: In H. K. Moffat (Ed.), *Topolog. Fluid Mechanics, Proceedings of the IUTAM Symposium*. Cambridge University Press.

Fredricks, R. W., & Coroniti, F. V. (1976). Ambiguities in the deduction of rest frame fluctuation spectrums from spectrums computed in moving frames. *Journal of Geophysical Research*, *81*, 5591–5595. https://doi.org/10.1029/ja081i031p05591

Frisch, U. (1995). *Turbulence. The legacy of A. N. Kolmogorov*. Cambridge: Cambridge University Press.

Hysell, D. L., Kelley, M. C., Swartz, W. E., Pfaff, R. F., & Swenson, C. M. (1986). Steepened structures in equatorial spread F: 1. new observations. *Journal of Geophysical Research*, *99*(A5), 8827–8840.

Ivarsen, M. F., Jin, Y., Spicher, A., & Clausen, L. B. N. (2019). Direct evidence for the dissipation of small-scale ionospheric plasma structures by a conductive E region. *Journal of Geophysical Research*, *124*, 2935–2942.

Jacobsen, K. S., Pedersen, A., Moen, J. I., & Bekkeng, T. A. (2010). A new Langmuir probe concept for rapid sampling of space plasma electron density. *Measurement Science and Technology*, *21*(8), 085902. https://doi.org/10.1088/0957-0233/21/8/085902

Jahn, J. M., & Labelle, J. (1998). Rocket measurements of high-altitude spread F irregularities at the magnetic dip equator. *Journal of Geophysical Research*, *103*(A10), 23427–23441. https://doi.org/10.1029/97ja02636

Jenkins, G. M., & Watts, D. G. (1968). *Spectral analysis and its applications*. San Francisco, California: Holden-Day.

Kelley, M. C. (2009). *The earth's ionosphere plasma physics and electrodynamics* (2nd ed., p. 96). Cambridge: Cambridge University Press.

Kelley, M. C., Pfaff, R. F., Baker, K. D., Ulwick, J. C., Livingston, R., Rino, C., & Tsunoda, R. (1982). Simultaneous rocket probe and radar measurements of equatorial spread F—Transitional and short wavelength results. *Journal of Geophysical Research*, *87*(A3), 1575–1588. https://doi.org/10.1029/ja087ia03p01575

Keskinen, M., & Ossakow, S. L. (1983). Theories of high-latitude ionospheric irregularities: A review. *Radio Science*, *18*(6), 1077–1091. https://doi.org/10.1029/rs018i006p01077

Keskinen, M. J., Mitchell, H. G., Fedder, J. A., Satyanarayana, P., Zalesak, S. T., & Huba, J. D. (1988). Nonlinear evolution of the Kelvin-Helmholtz instability in the high-latitude ionosphere. *Journal of Geophysical Research*, *93*(A1), 137–152. https://doi.org/10.1029/ja093ia01p00137

Kintner, P. M., & Seyler, C. E. (1985). The status of observations and theory of high-latitude ionospheric and magnetospheric plasma turbulence. *Space Science Reviews*, *41*(1–2), 91–129. https://doi.org/10.1007/bf00241347

Kolmogorov, A. N. (1941). Dissipation of energy in locally isotropic turbulence. *Doklady Akademii Nauk*, *32*(16).

LaBelle, J., Kelley, M. C., & Seyler, C. E. (1986). An analysis of the role of drift waves in equatorial spread F. *Journal of Geophysical Research*, *91*(A5), 5513–5525. https://doi.org/10.1029/ja091ia05p05513

Leamon, R. J., Smith, C. W., Ness, N. F., Matthaeus, W. H., & Wong, H. K. (1998). Observational constraints on the dynamics of the interplanetary magnetic field dissipation range. *Journal of Geophysical Research*, *103*(A3), 4775–4787. https://doi.org/10.1029/97ja03394

Linson, L. M., & Workman, J. B. (1970). Formation of striations in ionospheric plasma clouds. *Journal of Geophysical Research*, *75*(16), 3211–3219. https://doi.org/10.1029/ja075i016p03211

Lorentzen, D. A., Moen, J. I., Oksavik, K., Sigernes, F., Saito, Y., & Johnsen, M. G. (2010). In situ measurement of a newly created polar cap patch. *Journal of Geophysical Research*, *115*, A12323. https://doi.org/10.1029/2010ja015710

Matthaeus, W. H., Dasso, S., Weygand, J. M., Milano, L. J., Smith, C. W., & Kivelson, M. G. (2005). Spatial correlation of solar-wind turbulence from two-point measurements. *Physical Review Letters*, *95*(23), 231101. https://doi.org/10.1103/physrevlett.95.231101

Matthaeus, W. H., & Goldstein, M. L. (1982). Measurement of the rugged invariants of magnetohydrodynamic turbulence in the solar wind. *Journal of Geophysical Research*, *87*(16), 6011–6028. https://doi.org/10.1029/ja087ia08p06011

Moen, J. I., Carlson, H. C., Milan, S. E., Shumilov, N., Lybekk, B., Sandholt, P. E., & Lester, M. (2000). On the collocation between dayside auroral activity and coherent HF radar backscatter. *Annals of Geophysics*, *18*(12), 1531–1549. https://doi.org/10.1007/s00585-001-1531-2

Moen, J. I., Oksavik, K., Abe, T., Lester, M., Saito, Y., Bekkeng, T. A., & Jacobsen, K. S. (2012). First in-situ measurements of HF radar echoing targets. *Geophysical Research Letters*, *39*, L07104. https://doi.org/10.1029/2012gl051407

Moen, J. I., Oksavik, K., Alfonsi, L., Daabakk, Y., Romano, V., & Spogli, L. (2013). Space weather challenges of the polar cap ionosphere. *Journal of Space Weather and Space Climate*, *3*(A02), 13. https://doi.org/10.1051/swsc/2013025

Moen, J. I., Walker, I. K., Kersley, L., & Milan, S. E. (2002). On the collocation between dayside auroral activity and coherent HF radar backscatter. *Journal of Geophysical Research Letters*, *107*(A4), 1044. https://doi.org/10.1029/2001ja000111

Mounir, H., Cerisier, J. C., Berthelier, A., Lagoutte, D., & Béghin, C. (1991). The small-scale turbulent structure of the high-latitude ionosphere: ARCAD-AUREOL-3 observations. *Annales Geophysicae*, *9*, 725–737.

Oksavik, K., Moen, J. I., Lester, M., Bekkeng, T. A., & Bekkeng, J. K. (2012). In situ measurements of plasma irregularity growth in the cusp ionosphere. *Journal of Geophysical Research*, *117*(A11), A11301. https://doi.org/10.1029/2012ja017835

Pécseli, H. L. (2000). *Fluctuations in physical systems*. Cambridge, UK: Cambridge Univ. Press.

Pope, S. (2000). *Turbulent flows*. Cambridge, UK: Cambridge University Press.

Rinne, Y., Moen, J. I., Oksavik, K., & Carlson, H. C. (2007). Reversed flow events in the winter cusp ionosphere observed by the European Incoherent Scatter (EISCAT) Svalbard radar. *Journal of Geophysical Research*, *112*, A10313. https://doi.org/10.1029/2007ja012366

Sorriso-Valvo, L., Carbone, V., Veltri, P., Consolini, G., & Bruno, R. (1999). Intermittency in the solar wind turbulence through probability distribution functions of fluctuations. *Geophysical Research Letters*, *26*(13), 1801–1804. https://doi.org/10.1029/1999gl900270

Spicher, A., Deshpande, K., Jin, Y., Oksavik, K., Zettergren, M. D., Clausen, L. B. N., & Baddeley, L. (2020). On the production of ionospheric irregularities via Kelvin-Helmholtz instability associated with cusp flow channels. *Journal of Geophysical Research*, *125*(6), e2019JA027734. https://doi.org/10.1029/2019ja027734

Spicher, A., Ilyasov, A. A., Miloch, W. J., Chernyshov, A. A., Clausen, L. B. N., Moen, J. I., & Saito, Y. (2016). Reverse flow events and small-scale effects in the cusp ionosphere. *Journal of Geophysical Research: Space Physics*, *121*(10), 466–480. https://doi.org/10.1002/2016ja022999

Spicher, A., Miloch, W. J., Clausen, L. B. N., & Moen, J. I. (2015). Plasma turbulence and coherent structures in the polar cap observed by the ICI-2 sounding rocket. *Journal of Geophysical Research*, *120*(10), 959–978. https://doi.org/10.1002/2015ja021634

Spicher, A., Miloch, W. J., & Moen, J. I. (2014). Direct evidence of double-slope power spectra in the high-latitude ionospheric plasma. *Geophysical Research Letters*, *41*, 1406–1412. https://doi.org/10.1002/2014gl059214

Sreenivasan, K. R., & Antonia, R. A. (1997). The phenomenology of small-scale turbulence. *Annual Review of Fluid Mechanics*, *29*, 435–472. https://doi.org/10.1146/annurev.fluid.29.1.435

Tam, S. W. Y., Chang, T., Kintner, P. M., & Klatt, E. (2005). Intermittency analyses on the SIERRA measurements of the electric field fluctuations in the auroral zone. *Geophysical Research Letters*, *32*, L05109. https://doi.org/10.1029/2004gl021445

Taylor, G. I. (1938). The spectrum of turbulence. *Proceedings of the Royal Society A*, *164*, 476–490. https://doi.org/10.1098/rspa.1938.0032

Torrence, C., & Compo, G. P. (1988). A practical guide to wavelet analysis. *Bulletin of the American Meteorological Society*, *79*, 61–78.

Treuman, R. A., & Baumjohann, W. (1997). *Advanced space plasma physics*. UK: Imperial College Press.

Tsunoda, R. T. (1988). High-latitude F region irregularities: A review and synthesis. *Reviews of Geophysics*, *26*(4), 719–760. https://doi.org/10.1029/rg026i004p00719

Tu, C. Y., & Marsch, E. (1995). MHD structures, waves and turbulence in the solar wind: Observations and theories. *Space Science Reviews*, *73*(1), 1–210. https://doi.org/10.1007/bf00748891

Tu, C. Y., Roberts, D. A., & Goldstein, M. L. (1989). Spectral evolution and cascade constant of solar wind Alfénic turbulence. *Journal of Geophysical Research*, *94*(13), 575–578. https://doi.org/10.1029/ja094ia10p13575

Villain, J. P., Hanuise, C., & Beghin, C. (1986). ARCAD3-SAFARI coordinated study of auroral and polar F-region ionospheric irregularities. *Annales Geophysicae*, *4*, 841–853.